The chemistry of negotiation: Rhythmic, glycan-driven acidification in a symbiotic conversation

Julia A. Schwartzman, Eric Koch, Elizabeth A. C. Heath-Heckman[1], Lawrence Zhou, Natacha Kremer[2], Margaret J. McFall-Ngai, and Edward G. Ruby[3]

Department of Medical Microbiology and Immunology, University of Wisconsin–Madison, Madison, WI 53706

Edited by Caroline S. Harwood, University of Washington, Seattle, WA, and approved December 5, 2014 (received for review September 25, 2014)

Glycans have emerged as critical determinants of immune maturation, microbial nutrition, and host health in diverse symbioses. In this study, we asked how cyclic delivery of a single host-derived glycan contributes to the dynamic stability of the mutualism between the squid *Euprymna scolopes* and its specific, bioluminescent symbiont, *Vibrio fischeri*. *V. fischeri* colonizes the crypts of a host organ that is used for behavioral light production. *E. scolopes* synthesizes the polymeric glycan chitin in macrophage-like immune cells called hemocytes. We show here that, just before dusk, hemocytes migrate from the vasculature into the symbiotic crypts, where they lyse and release particulate chitin, a behavior that is established only in the mature symbiosis. Diel transcriptional rhythms in both partners further indicate that the chitin is provided and metabolized only at night. A *V. fischeri* mutant defective in chitin catabolism was able to maintain a normal symbiont population level, but only until the symbiotic organ reached maturity (~4 wk after colonization); this result provided a direct link between chitin utilization and symbiont persistence. Finally, catabolism of chitin by the symbionts was also specifically required for a periodic acidification of the adult crypts each night. This acidification, which increases the level of oxygen available to the symbionts, enhances their capacity to produce bioluminescence at night. We propose that other animal hosts may similarly regulate the activities of epithelium-associated microbial communities through the strategic provision of specific nutrients, whose catabolism modulates conditions like pH or anoxia in their symbionts' habitat.

symbiosis | squid–vibrio | metabolism | chitin

Animals exist in a microbial world and are reliant on beneficial associations with certain microbes for nutrition, defense, development, or other fitness factors (1). In the case of horizontally acquired symbioses, such as that in the gut, the success of the association hinges on the ability of microbial symbionts to colonize, be nourished by, and deliver a fitness advantage to the host, while maintaining a détente with its immune system (2–4). The negotiations underlying such mutually beneficial relationships must initiate upon first contact and continue throughout the period of association (5).

Three hallmarks of host–microbe interaction emerge from studies of the complex microbial consortia of animals. First, the provision of nutrients such as host-derived glycans contributes to the microbial community structure and is a source of microbe-derived metabolites such as short-chained fatty acids (SCFA) that promote the maturation of local and systemic immune functions (6–9). Second, the nutritional and environmental changes that mark the developmental trajectory of an organism from its juvenile to adult form are accompanied by distinct shifts in both the composition and functions of the maturing host's microbiota (10, 11). Finally, circadian rhythms coordinate much of the communication between a host and its microbiota, leading to the maintenance of physiological homeostasis (12–14). Taken together, these themes indicate that the terms of a protracted symbiotic negotiation are subject to a dynamic equilibrium that encompasses nutritional, immune, developmental, and circadian inputs.

Given this complexity, the specific costs incurred and benefits derived from a long-term cooperation, as well as their underlying mechanisms, are often difficult to establish, particularly in symbioses where the microbial member provides nutrients to the host. Natural invertebrate model systems that maintain one or a few symbiotic microbial species, such as nematodes, medicinal leeches, and squid (15), provide a window through which we can discover themes conserved across the diversity of interactions of animals with their coevolved microbiota, whether simple or complex. In particular, the symbiosis of the bobtail squid *Euprymna scolopes* and the luminous bacterium *Vibrio fischeri*, in which the microbial symbiont can be manipulated without compromising the health of the host, presents a rare opportunity to study the chemical and immune dialogues of symbiotic partners at a cellular and molecular level (16).

The squid–vibrio symbiosis occurs within the light-emitting organ of *E. scolopes* and is based on the bacterium's production of bioluminescence (17), which the host uses in its nocturnal behaviors, such as foraging and camouflage. The symbionts are obtained through horizontal transmission from the ambient seawater by each generation of juvenile squid (18) and are cultured in the epithelium-lined crypts of the light organ (Fig. 1*A*)

Significance

The chemical dialog through which a host promotes long-term symbioses with particular microbial partners remains largely unexplored, especially within complex consortia like the human microbiota. Natural, monospecific associations, including that between bobtail squid and *Vibrio fischeri*, have proved useful for discovering shared strategies, such as rhythmic microbial signaling and symbiosis-induced development, subsequently found in mammalian associations. Here, we demonstrate that symbiont metabolism is driven by a diel provision of a squid-derived glycan, resulting in tissue acidification. This event alters bacterial physiology, favoring the cyclic production of bioluminescence, the functional basis of the symbiosis. More generally, studies of this association can help reveal mechanisms by which other hosts modulate the chemistry of symbiosis to regulate microbial community function.

Author contributions: J.A.S., E.A.C.H.-H., M.J.M.-N., and E.G.R. designed research; J.A.S., E.K., E.A.C.H.-H., and L.Z. performed research; E.K., E.A.C.H.-H., and N.K. contributed new reagents/analytic tools; J.A.S. analyzed data; and J.A.S., M.J.M.-N., and E.G.R. wrote the paper.

The authors declare no conflict of interest.

This article is a PNAS Direct Submission.

Data deposition: The sequence reported in this paper has been deposited in the GenBank database (accession no. KM592978).

[1]Present address: Department of Molecular and Cellular Biology, University of California, Berkeley, CA 94720.

[2]Present address: Laboratoire de Biométrie et Biologie Evolutive, UMR CNRS 5558, Université Lyon 1, Université de Lyon, 69622 Villeurbane Cédex, France.

[3]To whom correspondence should be addressed. Email: egruby@wisc.edu.

This article contains supporting information online at www.pnas.org/lookup/suppl/doi:10.1073/pnas.1418580112/-/DCSupplemental.

throughout the animal's ~9-mo life. The symbiont induces post-embryonic light-organ development (19), and the organ morphology reaches maturity in 4 wk (20). Host-derived chitin, a polymeric glycan of *N*-acetylglucosamine, is known to promote the species-specific colonization of the squid by *V. fischeri* (21). Chitin is synthesized by several types of squid tissue, including macrophage-like immune cells called hemocytes (22) (Fig. 1*A*), and has also been implicated, along with amino acids (23), as a nutrient provided to the symbiont population. Specifically, transcription of *V. fischeri* genes associated with the fermentation of chitin oligosaccharides (COS) is elevated during the nocturnal, bioluminescent phase of the symbiosis (24) (Fig. 1*A*). The importance of chitin in the chemical dialogue between squid and vibrio is reminiscent of the contribution of host glycans and structural polysaccharides to other host–microbe interactions (9). For example, (*i*) the catabolism of exoskeleton-derived chitin by *Vibrio cholerae* enhances transmission from an invertebrate vector to a susceptible host (25), (*ii*) pectin catabolism by the plant pathogen *Xylella fastidiosa* promotes transmission to leafhopper vectors (26), and (*iii*) foraging of mammalian mucin-derived glycans, such as fucose and sialic acid, forms a nutritional scaffold for the gut microbiota (27–29).

The squid–vibrio association is also characterized by daily rhythms of symbiont growth and bioluminescence (30, 31). Each morning at dawn, the host expels the contents of the light-organ crypts, including 95% of the symbiont population, into the surrounding seawater (Fig. 1*A*). The remaining symbiont cells repopulate the light organ within hours, by growing on substrates including amino acids and glycerophospholipids (23, 24), eventually providing the squid's nocturnal bioluminescence. Light emission, which requires oxygen (32), is highest during the night (33). In the fully developed light organ, where the symbionts are oxygen limited (24, 33), the diel bioluminescent rhythm is potentiated by an acidic crypt environment, which creates a Bohr effect that releases oxygen from the carrier protein, hemocyanin (34). Here, we demonstrate that, in this mature state of light-organ development, the cyclic provision of COS to symbionts, combined with their fermentation of this glycan, leads to the nightly acidification of the symbiont-containing extracellular crypts. The combined nocturnal activities of host and symbiont thereby promote the diel cycle of bioluminescence: a rhythm critical to the long-term stability of this association.

Results and Discussion

Hemocytes Deliver Chitin to the Light Organ. The diel transcription of chitin-utilization genes by symbiotic *V. fischeri* (24), together with the presence of chitin within the host's macrophage-like hemocytes (22), suggests that the hemocytes convey this nutrient to the symbionts. To test this hypothesis, we first characterized the distribution of chitin in the light organ's central core. Two major host cell types compose this tissue: the polarized microvillar epithelium that defines the symbiont-containing crypt spaces and the hemocytes that migrate into them (Fig. 1*A*). We collected samples of central core tissue at dusk [10 h postdawn (hpd), Fig. 1*A*] and just before dawn (22 hpd, Fig. S1*A*) and probed for the presence of particulate chitin. Fluorescently labeled chitin-binding protein (CBP) colocalized almost exclusively with the hemocyte-specific, cytoplasmic marker, DNase-I (Fig. 1*B*). Importantly, although soluble COS molecules (which do not bind CBP) may exist elsewhere, our observations support the idea that hemocytes are the main cell type within the light organ that contains particulate chitin.

Our previous observations of the contents of the light-organ crypts suggested that both live and dead hemocytes are present among the densely packed symbiotic bacteria (35). Thus, we hypothesized that chitin particles are delivered to the symbiont population by the death and lysis of chitin-containing hemocytes that have migrated into the crypts. A more extensive examination of crypt contents released at night (22 hpd) revealed two kinds of

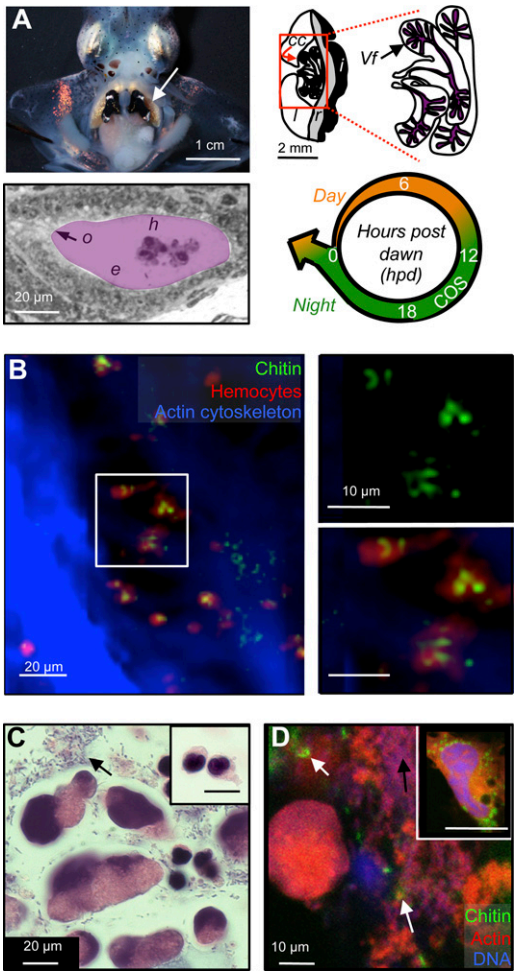

Fig. 1. Light-organ crypts contain hemocyte-derived chitin. (*A*) Anatomy of the mature light organ. (*Top Left*) The mature, bilobed light organ is located ventrally, in the center of the mantle cavity (arrow). (*Top Right*) Schematic of one lobe, indicating the light-organ lens (l), reflector (r), and ink sac (i), as well as the bacteria-containing central-core tissue (cc) in the red box. Polarized epithelial cells form branched crypt spaces, in which the symbionts (*Vf*) reside. (*Bottom Left*) Symbiotic *V. fischeri* cells occupy extracellular crypts (purple), where they contact hemocytes (*h*) and the bordering epithelial cells (*e*); the outlet (*o*) to the mantle cavity allows the host to expel most of the crypt contents and symbionts every morning at dawn. (*Bottom Right*) The diel cycle of the mature squid–vibrio symbiosis. Throughout the animal's life, about 95% of the symbiont population is expelled at dawn (arrow), and the remaining cells repopulate the crypts during the day (orange). At night (green), transcriptional evidence in the mature symbiosis suggests that symbionts metabolize host-derived chitin oligosaccharides (COS) (24) and produce luminescence. Numbers indicate hours post dawn (hpd). (*B*) Confocal micrograph, showing colocalization of chitin (fluorescent chitin-binding protein; green) and hemocytes (fluorescent DNase-I globular actin-binding protein; red) in central-core tissue (fluorescent phalloidin, a filamentous actin-binding protein; blue). Image is a 3D reconstruction of 40 1-μm confocal sections. Tissue was sampled just before nightfall (10 hpd). (*Top Right* and *Bottom Right*) Close-up of hemocytes in white box, highlighting particulate-chitin staining. (*C*) Differential interference contrast micrograph of crypt contents, sampled at the end of the night (22 hpd) and stained with hematoxylin (chromatin; dark blue), and eosin (proteins; pink). Two different morphologies of nucleated cells are seen in the crypt contents. *Inset* (same magnification) shows the single type of hemocyte morphology present in the hemolymph. Black arrow indicates extracellular material, which includes bacterial cells. (*D*) Detection of free particulate chitin (white arrows) and extracellular material (black arrows, here and in *C*) in the contents of the light-organ crypt, sampled 22 hpd. Fluorescent staining is as in *B*. *Inset* shows image of cytoplasmic particulate chitin within a hemocyte extracted from the hemolymph.

host cells: (*i*) compact 10-μm diameter cells and (*ii*) ~20-μm variable-diameter cells with diffuse DNA staining, ruptured acidic vacuoles, and irregular membrane morphology (Fig. 1*C* and Fig. S1*B*), consistent with living and moribund hemocytes, respectively. The presence of the latter morphology in the nocturnal crypts raised the question of whether exposure to the conditions present in this environment (34) was sufficient to cause hemocyte damage.

When we suspended healthy hemocytes derived from hemolymph (pH ~7) for 1 h in crypt contents buffered at either pH 7.5 or the nocturnal crypt pH of 5.5 (34), the initially intact hemocytes swelled, produced membrane blebs, and showed a loss of integrity of their acidic vacuoles (Fig. S1*C*). If the crypt contents were heat treated, they elicited the same effect. Thus, a heat-resistant, neutral-pH active, component of the crypt contents can trigger a change in hemocyte appearance that is consistent with hemocyte damage. In addition, when crypt contents were collected 2 h before dawn (22 hpd) and probed with CBP, we observed healthy-looking cells that contained particles of chitin, free chitin in the extracellular crypt matrix, and moribund cells morphologically similar to those observed in the in vitro studies described above (Fig. 1*D*). Collectively, the data are consistent with a model wherein chitin particles within host hemocytes are released into the crypts and become accessible to extracellular hydrolysis by both host and symbiont chitinases (21, 24, 36).

Symbiont-Dependent Hemocyte Trafficking into the Light Organ Is on a Diel Cycle. For hemocytes to deliver COS to symbionts only during the nocturnal phase of the diel cycle, some aspect of their behavior must be rhythmic. We have previously reported a symbiosis-induced increase in the number of hemocytes associated with the light organ in immature, 2-d-old squid (37). We extended this observation by asking whether the increase in hemocytes was dependent on the time of day and, thus, a symbiosis-dependent diel migratory rhythm. Consistent with previous results (37), approximately four times more hemocytes were found in symbiotic than in aposymbiotic light organs of 2-d-old squid at dusk (10 hpd, Fig. 2*A*). However, we noted that this increase was transient: The number of hemocytes in symbiotic light organs returned to aposymbiotic levels by the end of the night (22 hpd), and no accumulation of hemocytes was noted in the crypts of the immature light organs. This pattern of hemocyte migration recurred the following day (Fig. S2*A*), demonstrating that the migration into symbiotic light organs at dusk is likely a diel pattern, rather than a single event in the trajectory of an immunological and/or developmentally triggered response to colonization. Thus, a symbiosis-dependent diel rhythm of hemocyte migration is established within the first few days following light-organ colonization.

We next investigated whether a similar rhythm of hemocyte migration occurred in mature light organs. At this stage of development, transcription of the predicted *E. scolopes* chitotriosidase gene *eschit1* exhibits a diel periodicity, with expression highest at night (24). This gene is also transcribed by hemocytes (22). Western-blot analysis demonstrated that the chitotriosidase enzyme itself was present in central core tissue; i.e., the *Es*Chit1 antibody (α-*Es*Chit1) hybridized to a 50-kDa band (the molecular mass predicted for *Es*Chit1), as well as two smaller bands in the soluble fraction of central-core proteins (Fig. 2*B*). This multiband pattern is consistent with the posttranslational processing that occurs during the activation of invertebrate chitinases (38). In addition, fluorescence immunocytochemistry and confocal microscopy of the central core localized the *Es*Chit1 protein exclusively to the hemocytes found there (Fig. 2*C*). We confirmed these observations by isolating hemocytes and probing them directly for *Es*Chit1: Cells from both mature and immature animals exhibited α-*Es*Chit1-positive puncta (Fig. 2*D* and Fig. S2*B*), irrespective of symbiotic state. Thus, hemocytes express the majority of *Es*Chit1 in light organ tissue, and *eschit1* transcript can be associated with the presence of hemocytes.

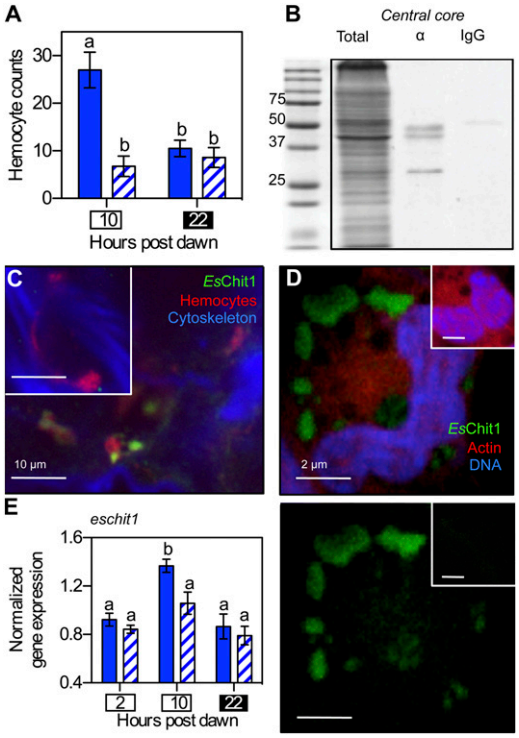

Fig. 2. The diel migration of hemocytes to the light organ is symbiont dependent. (*A*) Enumeration of hemocytes present during the day (10 hpd; white box) and night (22 hpd; black box) in light-organ tissues of 2-d-old, immature symbiotic (solid bars) or aposymbiotic (hatched bars) animals. n = 15 light organs, error bars indicate SEM, and data are representative of three independent experiments. "a" and "b" indicate groups of statistically similar means, determined with two-way ANOVA with post hoc Bonferroni *T*-tests. (*B*) Western blot showing presence of *Es*Chit1 in 25 μg of total soluble protein isolated from light-organ central cores. Total, total soluble protein; α, anti-*Es*Chit1 antibody; IgG, Ig control. (*C*) Confocal micrograph localizing *Es*Chit1 in whole adult (>4-wk-old) central cores at dusk (10 hpd). *Inset* shows preimmune control. (*D*) Localization of *Es*Chit1 in hemocytes extracted from adult symbiotic squid. (*Bottom*) Anti-*Es*Chit1 signal alone; (*Top*) anti-*Es*Chit1 signal merged with rhodamine phalloidin (filamentous actin specific) and TOTO-3 (DNA specific). *Insets* show preimmune control. (*E*) Diel pattern of the transcription of host chitotriosidase (*eschit1*) in adult symbiotic (solid bars) and aposymbiotic (hatched bars) light organs; error bars indicate SEM, n = 5; statistical tests are as described in *A*.

To determine whether the diel rhythm of *eschit1* transcription originally observed in mature central-core tissues occurred only in the symbiotic state, we profiled the transcript levels of this gene at three times of day, in both symbiotic and aposymbiotic mature light organs, by quantitative real-time PCR. Consistent with previous results (24), hemocyte-associated *eschit1* transcript levels increased significantly in mature symbiotic light organs just before nightfall (10 hpd, Fig. 2*E*). This increase was not observed in aposymbiotic light organs, although transcript levels were comparable between the two groups, both in the morning and at the end of the night (2 hpd and 22 hpd, respectively) (Fig. 2*E*). Transcription of another, functionally distinct, hemocyte-associated *E. scolopes* gene, peptidoglycan-recognition protein 5 (*espgrp5*) (39), displayed the same symbiont-dependent peak at dusk as *eschit1* (Fig. S2*C*). This pattern in hemocyte-associated transcripts mirrors the transient, symbiosis-dependent increase in hemocyte numbers observed in immature light organs and is consistent with a nightly hemocyte migration into the crypts of mature light organs, although it may also indicate a small symbiosis-dependent induction of these two genes as well. Although we do not know whether this rhythmic migration has circadian

MICROBIOLOGY

underpinnings, in vertebrates, macrophages migrate into tissues as part of a circadian cycle that is entrained by microbial cues (13).

Delivery of COS to the Symbionts Begins in the Mature Light Organ. We next asked whether the symbionts metabolize COS and, if so, what consequences it might have for the association. To investigate COS metabolism within the crypts, we constructed a mutant strain of *V. fischeri* that would act as a biosensor. Catabolism of chitin (Fig. 3*A*) is a general characteristic of the Vibrionaceae, and this glycan is an important environmental nutrient and cue for both beneficial and pathogenic species in this family (25). To construct the COS biosensor, we deleted the *V. fischeri nagB* gene, which encodes glucosamine deaminase: the final enzymatic step by which COS and other amino sugars enter the central carbon metabolism of *V. fischeri* (36). Such a mutant cannot grow on this group of sugars (Fig. 3*A* and Fig. S3*A*). As with the homologous *Escherichia coli* mutant (40), in a complex growth medium, *V. fischeri ΔnagB* was sensitive to 100 μM of the COS monomer *N*-acetyl glucosamine (GlcNAc), a level even below that required for significant growth (Fig. S3*B*). As expected, this sensitivity was eliminated by genetically complementing the *ΔnagB* strain *in cis* at the Tn*7* site on the *V. fischeri* chromosome, a neutral site for integration of DNA elements (41) (Fig. 3*B*). The effect of COS on *ΔnagB* growth was also relieved by the presence of a nongluconeogenic sugar of the pentose-phosphate pathway (e.g., fructose, glucose, or ribose; Fig. S3*C*), confirming that the growth-arrest phenotype is attributable to substrate inhibition (40).

From these observations, we reasoned that *V. fischeri ΔnagB* would have difficulty colonizing the squid light organ under two conditions: (*i*) where COS is present at a level sufficient to support wild-type growth or (*ii*) where there is even a small amount of COS (e.g., ~100 μM), but no ameliorating pentose-phosphate pathway sugars. We compared colonization levels in light organs populated by either wild-type or *ΔnagB* strains of *V. fischeri* during the first 4 wk postcolonization to determine when symbionts might encounter such environments (Fig. 3*C*). For at least 2 wk, squid were colonized equally well by wild-type or *ΔnagB* cells; however, by 4 wk, light organs colonized by the *ΔnagB* strain contained <15% as many symbiont cells as those colonized by either wild type or the *in cis* complemented strain (Fig. 3*C*). The *ΔnagB* strain showed no decrease in fitness during cocolonization with wild type throughout a 4-wk colonization (Fig. S3*D*), probably due to an effective lowering of the ambient COS concentration by wild-type metabolism. Similarly, coculture of *ΔnagB* and wild-type *V. fischeri* allowed growth of the mutant, even in the presence of up to 2.5 mM GlcNAc (Fig. S3*E*), suggesting that the concentration of COS available to symbionts in the light organ never exceeds a few millimolar. Although we cannot rule out the possibility that COS are present in the immature light-organ crypt at a level below the sensitivity of our biosensor strain (i.e., 10–100 μM), our data do indicate that COS catabolism emerges as a major metabolic strategy for symbiotic *V. fischeri* between 2 wk and 4 wk posthatch. These data also indicate that the presence of COS in the light-organ crypts is not directly linked to the squid's diet: The squid consumes a chitin-rich diet throughout the rearing process. The developmental, diet-independent, regulation of COS availability echoes the life stage-specific presentation of surface sugars to glycan-foraging microbes during mammalian gut development (27).

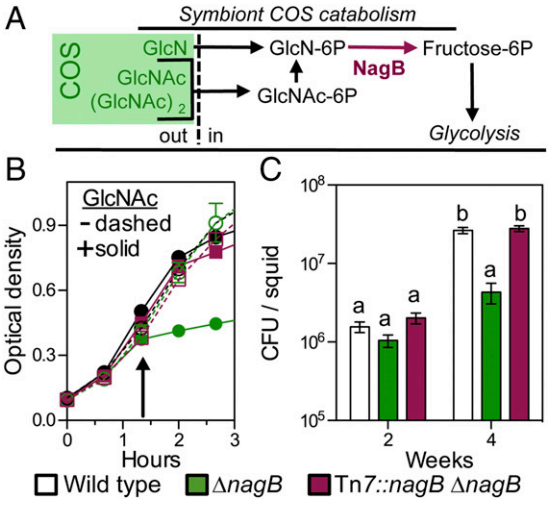

Fig. 3. Symbionts sense chitin oligosaccharides (COS) only in the mature light organ. (*A*) Catabolism of COS in the genus *Vibrio*. COS are derivatives of amino di- and monosaccharides that represent enzymatic products of chitin hydrolysis (green box). After the COS are transported into the cell as the phosphorylated form, the acetyl and amino groups are removed from the hexose core before it enters glycolysis. The last common step in COS catabolism is the deamination of glucosamine-P by the enzyme NagB. To define amino sugar and COS catabolism in *V. fischeri*, we tested the ability of the *ΔnagB* mutant to grow on several sugars as a sole source of carbon (data shown in Fig. S3*A*). GlcNAc, *N*-acetyl glucosamine; $(GlcNAc)_2$, *N*-acetylchitobiose; GlcN, glucosamine; out, extracellular or periplasmic space; in, intracellular space. (*B*) Growth of a *ΔnagB V. fischeri* mutant in seawater–tryptone medium (SWTO), either without (–) or with (+) the addition of 20 mM GlcNAc at the arrow. Error bars indicate SEM, $n = 4$. (*C*) Extent of colonization of the squid light organ at immature and mature stages of host development by wild type, *ΔnagB*, and an *in cis* complemented (*ΔnagB* Tn*7::nagB)* strain. cfu, colony-forming units; error bars indicate SEM, $n = 12$; statistical tests on log-transformed data are as described in Fig. 2.

Catabolism of COS by the Symbionts Drives a Diel Cycle of Crypt Acidification. To determine whether the delivery of *E. scolopes* chitin, like that of mammalian glycans (27), shapes the ecology of the mature state of symbiosis, we asked whether the appearance of COS in the light-organ crypts induced any changes in symbiont physiology and/or the crypt environment. Catabolism of COS produces acetic acid in culture; thus, we performed a comparative study of COS catabolism, and associated acetate production, under aerobic culture conditions in four strains (Table S1): *V. fischeri* ES114 (the wild-type squid symbiont used in this study), *V. fischeri* MJ11 (a fish light-organ symbiont), *Vibrio harveyi* (a nonsymbiotic seawater isolate), and *E. coli* K-12 (an enteric strain found in the mammalian gut). When grown on either *N*-acetylglucosamine or glucose, the three *Vibrio* strains produced two to three times more acetate per unit growth, and more acetate per mole substrate, than did *E. coli*, suggesting that the aerobic catabolism of glycolytic substrates by *Vibrio* spp. relies more on substrate-level phosphorylation for energy generation than *E. coli* does. This excretion of acetate during aerobic growth is consistent with a metabolic imbalance called the Crabtree effect (42). In the context of the light-organ environment, the Crabtree effect would lead to the excretion of SCFA like acetate during growth on COS, thereby acidifying the crypt lumen and enhancing the allocation of ambient oxygen toward bioluminescence (34).

We reasoned that if SCFA accumulate as an excreted product of symbiont COS catabolism, they might cause acidification of the light-organ crypts. In a number of bacteria, including *V. fischeri* (Fig. S4*A*), exposure to low pH induces an acid-tolerance response (ATR) that mitigates a potentially lethal collapse of the cell's proton motive force by protonated weak acids like SCFA (43). As expected (Table S1), during COS catabolism in unbuffered media, wild-type *V. fischeri* excreted sufficient acetate to acidify the culture supernatant to pH 5.5, inducing an ATR; however, when the COS medium was strongly buffered at pH 7.5, there was no ATR (Fig. 4*A*). The *ΔnagB* mutant, which is impaired in COS metabolism, did not acidify even an unbuffered COS medium and, thus, failed to induce an ATR. In contrast, when grown on glucose, a NagB-independent, acid-generating source of carbon, this mutant

did reduce the pH and induce a robust ATR (Fig. S4*B*). Thus, we reasoned that the failure of the *ΔnagB* mutant to induce an ATR when COS is present was due to its inability to catabolize COS to acetate (Fig. 3*A*), rather than to causing a defect in the ATR mechanism itself.

We next used the ATR as a reporter to indicate whether symbiont catabolism of COS acidifies the light-organ crypts; specifically, we released *V. fischeri* cells from the light organ and immediately determined whether they had recently induced an ATR. Wild-type symbionts exhibited an ATR when released from the light organs of mature squid at night (18 hpd and 23 hpd, Fig. 4*B* and Fig. S4*C*), consistent with the acidic pH measured in crypt contents at night (34). In contrast, symbionts released in the morning (3 hpd) showed no evidence of ATR induction, even though they were physiologically capable of inducing this response if they were exposed to acidic conditions before the assay (Fig. 4*B*). In contrast, the *ΔnagB* strain of *V. fischeri* failed to exhibit an ATR when released from the mature light organ at night, indicating it had not experienced a low pH in the crypts (Fig. 4*C* and Fig. S4*C*). Wild-type symbionts released from immature (2-d-old) light organs, even at night, also showed no evidence of an ATR (Fig. 4*B* and Fig. S4*D*), consistent with the notion that the immature host does not provide its symbionts sufficient COS (or other fermentable carbon sources) to promote acidification.

To estimate the amount of symbiont acid production that would be needed to reduce the pH of the crypts to an ATR-inducing 5.5, we measured the buffering capacity of freshly isolated squid hemolymph. Hemolymph, which is the major constituent of the crypt environment (34), required the addition of ~7.5 mM acetic acid to reach a pH of 5.5 (Fig. S4*E*). The incomplete oxidation of a molecule of *N*-acetyl glucosamine produces at least one molecule of acetate (Table S1) and could stoichiometrically produce as many as three. Thus, a nightly catabolism by the symbiont population of a few millimolar COS would be sufficient to create the level of acidification measured in the adult light-organ crypts (*SI Calculations*).

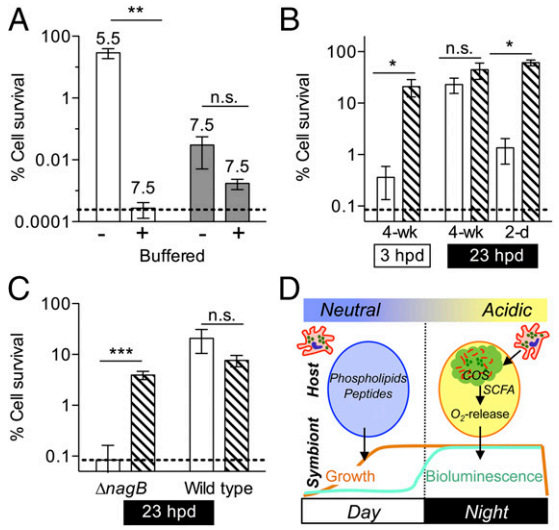

Fig. 4. Acidification due to COS catabolism is sufficient to induce the *V. fischeri* acid tolerance response in symbiosis. *V. fischeri* was exposed to different conditions before challenge with 40 mM short-chained fatty acid (SCFA) medium at pH 4.5. Survival (induction of an acid tolerance response, ATR) was evaluated after 20 min. ANOVAs with post hoc Bonferroni *T*-tests were performed on log-transformed data; error bars, SEM; dashed line, limit of detection; n.s., no significance, $*P < 0.05$, $**P < 0.01$, $***P < 0.01$. (*A*) Wild-type and *ΔnagB V. fischeri* were grown with 40 mM GlcNAc in either unbuffered or buffered medium (final culture pHs are indicated above bars) ($n = 6$). (*B*) Symbiotic wild-type *V. fischeri* was released from mature light organs during either the day (3 hpd) or the night (23 hpd). Alternately, symbionts were released from six individual pools of 20 2-d-old light organs at night (23 hpd). Released symbionts were assayed immediately for ATR (open bars) or after a period of preexposure to 30 mM SCFA medium at pH 5.5 (hatched bars) as a positive control ($n = 5$). (*C*) *ΔnagB* or wild-type *V. fischeri* were released from mature light organs at night (23 hpd). Symbionts were assayed for ATR either immediately following release (open bars), or after preexposure for 1 h (hatched bars) as in *B*, before acid killing ($n = 6$). (*D*) Model of diel metabolic cross-talk between the adult host and its symbionts. During the day, growth of symbionts on host-derived nutrients (peptides and phospholipids) in the crypt spaces (circles) is pH neutral (24). At dusk, hemocytes (red) migrate into the light-organ crypt lumen, lyse, and release chitin oligosaccharides (COS, green). The COS are catabolized by symbionts to produce SCFA, which acidify the crypt lumen and promote oxygen release (34). Oxygen fuels the enzymatic production of light by symbiont luciferase, the functional basis of the squid–vibrio mutualism.

Conclusions

Collectively, the data presented here support the hypothesis that (*i*) a nocturnal release of chitin from hemocytes in the light-organ crypts characterizes the mature diel cycle of the squid–vibrio symbiosis, (*ii*) symbiont catabolism of COS acidifies the crypt environment and induces the *V. fischeri* ATR at night, and (*iii*) this cycle is not active in the immature association, but develops only as the host matures (Fig. 4*D*). Previous work has shown that an acidic crypt pH potentiates the release of oxygen from hemocyanin (34) at the time when the symbiont's nocturnal light production increases (33). Thus, the host's cyclic provision of chitin, coupled with the symbionts' physiological responses to this rhythm, regulates the output of bioluminescence, the central product of the association (17). To acidify the light-organ crypts to their nighttime pH of ~5.5 (34) would require an amount of acetate released by catabolism of 11 μg of COS; we estimate that this amount of substrate could be transported into the crypts by ~2,000 hemocytes or 5% of the total circulating population (*SI Calculations*) (35, 44). The nightly sacrifice of this number of immune cells may appear to be a costly strategy for the host, and we cannot be certain that other, complementary mechanisms of COS delivery do not exist. However, 5% is less than the reported percentage of circulating hemocytes normally replaced by mollusks every few days (44), suggesting that the accumulation of a fraction of hemocytes in the crypt may be one strategy by which senescent cells are efficiently repurposed. Whether or not this strategy of delivering a specific glycan is costly to the host, if immune-cell derived chitin is the key that unlocks a nocturnal cycle of symbiont bioluminescence, then the sacrifice of a small fraction of its hemocytes may be a viable strategy for maintaining a stable, cooperative association.

pH homeostasis is emerging as a factor that regulates not only the phylogenetic composition of complex microbial communities in the oral cavity and gut, but also immune maturation and host health (45–47). In the squid–vibrio symbiosis, the diel acidification of the host tissue environment by bacterial metabolism is likely to affect activities beyond the bioluminescence phenotype of this association. The squid encodes homologs of zebrafish enzymes that inactivate immunogenic microbe-associated molecular pattern (MAMP) molecules. These enzymes lose activity at a low pH (48–51), suggesting that diel tissue acidification might lead to a local or systemic increase in MAMP levels at night. MAMPs promote the establishment of symbiosis by signaling pattern recognition receptors (PRRs) (8); thus, it is possible that acidification underlies a daily activation of PRR signal cascades. In addition, induction of bacterial acid tolerance has been associated with cross-protection and attenuation of immune-related antimicrobial compounds (52, 53). Consequently, an understanding of the mechanisms by which bacteria, whether beneficial or pathogenic, modulate the pH of colonized tissues is of critical importance to deciphering the molecular basis of these interactions.

Materials and Methods

See *SI Materials and Methods* for additional experimental details, including strains (Table S2) and primers (Table S3) used in this study, and the full sequence of *Es*Chit1 (Fig. S5).

ATR Assays. The induction of the *V. fischeri* ATR was monitored by assaying resistance to killing by exposure to a pH 4.5 mixture of SCFA for 20 min (54). To obtain symbiotic *V. fischeri* for the ATR assay, we collected a homogenate of either central-core tissues from individual adult (>4-wk-old) squid light organs or 50 whole juvenile (2-d-old) squid; both preparations were suspended at $\sim 10^7$ cfu/mL.

Detection of Chitin, and Immunocytochemistry. Chitin was detected in hemocytes and light-organ tissues, using commercially available FITC- or TRITC-conjugated CBP (New England Biolabs) (22). Light-organ tissues and hemocytes from the hemolymph of >4-wk-old squid, or whole tissue from 2-d-old light organs, were collected and prepared for immunocytochemistry (ICC) and confocal microscopy, using standard procedures (22, 48).

ACKNOWLEDGMENTS. We thank S. Nyholm, K. Vetsigian, R. Welch, H. Blackwell, and J. Reed for contributive discussions and Nell Bekiares and the Kewalo Marine Laboratory, University of Hawaii-Manoa, for support during animal experiments. This work was funded by NIH Grants RR12294/OD11024 (to E.G.R. and M.J.M.-N.) and AI050661 (to M.J.M.-N.). J.A.S. was funded by a National Science Foundation Graduate Research Fellowship, by the Chemical Biology Training Program [University of Wisconsin (UW)–Madison, NIH–National Institute of General Medical Sciences Grant T32 GM008505], and by the Microbes in Health and Disease Training Program (UW–Madison NIH–National Institute of Allergy and Infectious Diseases Grant T32 AI055397).

1. McFall-Ngai M, et al. (2013) Animals in a bacterial world, a new imperative for the life sciences. *Proc Natl Acad Sci USA* 110(9):3229–3236.
2. Schluter J, Foster KR (2012) The evolution of mutualism in gut microbiota via host epithelial selection. *PLoS Biol* 10(11):e1001424.
3. Hooper LV, Littman DR, Macpherson AJ (2012) Interactions between the microbiota and the immune system. *Science* 336(6086):1268–1273.
4. Kereszt A, Mergaert P, Maróti G, Kondorosi E (2011) Innate immunity effectors and virulence factors in symbiosis. *Curr Opin Microbiol* 14(1):76–81.
5. Axelrod R (1984) *The Evolution of Cooperation* (Basic Books, New York).
6. Lee W-J, Hase K (2014) Gut microbiota-generated metabolites in animal health and disease. *Nat Chem Biol* 10(6):416–424.
7. Maynard CL, Elson CO, Hatton RD, Weaver CT (2012) Reciprocal interactions of the intestinal microbiota and immune system. *Nature* 489(7415):231–241.
8. Gilbert SF (2014) A holobiont birth narrative: The epigenetic transmission of the human microbiome. *Front Genet* 5:282.
9. Chaston J, Goodrich-Blair H (2010) Common trends in mutualism revealed by model associations between invertebrates and bacteria. *FEMS Microbiol Rev* 34(1):41–58.
10. Nicholson JK, et al. (2012) Host-gut microbiota metabolic interactions. *Science* 336(6086):1262–1267.
11. Tremaroli V, Bäckhed F (2012) Functional interactions between the gut microbiota and host metabolism. *Nature* 489(7415):242–249.
12. Scheiermann C, Kunisaki Y, Frenette PS (2013) Circadian control of the immune system. *Nat Rev Immunol* 13(3):190–198.
13. Keller M, et al. (2009) A circadian clock in macrophages controls inflammatory immune responses. *Proc Natl Acad Sci USA* 106(50):21407–21412.
14. Mukherji A, Kobiita A, Ye T, Chambon P (2013) Homeostasis in intestinal epithelium is orchestrated by the circadian clock and microbiota cues transduced by TLRs. *Cell* 153(4):812–827.
15. Mandel MJ (2010) Models and approaches to dissect host-symbiont specificity. *Trends Microbiol* 18(11):504–511.
16. McFall-Ngai MJ (2014) The importance of microbes in animal development: Lessons from the squid-vibrio symbiosis. *Annu Rev Microbiol* 68(1):177–194.
17. Stabb EV, Visick KL (2013) *Vibrio Fisheri: Squid Symbiosis. The Prokaryotes* (Springer, New York), pp 497–532.
18. McFall-Ngai M, Heath-Heckman EA, Gillette AA, Peyer SM, Harvie EA (2012) The secret languages of coevolved symbioses: Insights from the *Euprymna scolopes-Vibrio fischeri* symbiosis. *Semin Immunol* 24(1):3–8.
19. Doino JA, McFall-Ngai M (1995) A transient exposure to symbiosis-competent bacteria induces light organ morphogenesis in the host squid. *Biol Bull* 189:347–355.
20. Koch EJ, Miyashiro T, McFall-Ngai MJ, Ruby EG (2014) Features governing symbiont persistence in the squid-vibrio association. *Mol Ecol* 23(6):1624–1634.
21. Kremer N, et al. (2013) Initial symbiont contact orchestrates host-organ-wide transcriptional changes that prime tissue colonization. *Cell Host Microbe* 14(2):183–194.
22. Heath-Heckman EA, McFall-Ngai MJ (2011) The occurrence of chitin in the hemocytes of invertebrates. *Zoology* 114(4):191–198.
23. Graf J, Ruby EG (1998) Host-derived amino acids support the proliferation of symbiotic bacteria. *Proc Natl Acad Sci USA* 95(4):1818–1822.
24. Wier AM, et al. (2010) Transcriptional patterns in both host and bacterium underlie a daily rhythm of anatomical and metabolic change in a beneficial symbiosis. *Proc Natl Acad Sci USA* 107(5):2259–2264.
25. Meibom KL, et al. (2004) The *Vibrio cholerae* chitin utilization program. *Proc Natl Acad Sci USA* 101(8):2524–2529.
26. Killiny N, Almeida RP (2009) Host structural carbohydrate induces vector transmission of a bacterial plant pathogen. *Proc Natl Acad Sci USA* 106(52):22416–22420.
27. Koropatkin NM, Cameron EA, Martens EC (2012) How glycan metabolism shapes the human gut microbiota. *Nat Rev Microbiol* 10(5):323–335.
28. Ng KM, et al. (2013) Microbiota-liberated host sugars facilitate post-antibiotic expansion of enteric pathogens. *Nature* 502(7469):96–99.
29. Kashyap PC, et al. (2013) Genetically dictated change in host mucus carbohydrate landscape exerts a diet-dependent effect on the gut microbiota. *Proc Natl Acad Sci USA* 110(42):17059–17064.
30. Heath-Heckman EA, et al. (2013) Bacterial bioluminescence regulates expression of a host cryptochrome gene in the squid-Vibrio symbiosis. *MBio* 4(2):e00167-13.
31. Lee KH, Ruby EG (1994) Effect of the squid host on the abundance and distribution of symbiotic *Vibrio fischeri* in nature. *Appl Environ Microbiol* 60(5):1565–1571.
32. Dunn AK (2012) *Vibrio fischeri* metabolism: Symbiosis and beyond. *Adv Microb Physiol* 61:37–68.
33. Boettcher K, Ruby E, McFall-Ngai M (1996) Bioluminescence in the symbiotic squid *Euprymna scolopes* is controlled by a daily biological rhythm. *J Comp Physiol* 179(1): 65–73.
34. Kremer N, et al. (2014) The dual nature of haemocyanin in the establishment and persistence of the squid-vibrio symbiosis. *Proc Biol Sci* 281(1785):20140504.
35. Nyholm SV, McFall-Ngai MJ (1998) Sampling the light-organ microenvironment of *Euprymna scolopes*: Description of a population of host cells in association with the bacterial symbiont *Vibrio fischeri*. *Biol Bull* 195(2):89–97.
36. Miyashiro T, et al. (2011) The *N*-acetyl-D-glucosamine repressor NagC of *Vibrio fischeri* facilitates colonization of *Euprymna scolopes*. *Mol Microbiol* 82(4):894–903.
37. Koropatnick TA, Kimbell JR, McFall-Ngai MJ (2007) Responses of host hemocytes during the initiation of the squid-Vibrio symbiosis. *Biol Bull* 212(1):29–39.
38. Renkema GH, et al. (1997) Synthesis, sorting, and processing into distinct isoforms of human macrophage chitotriosidase. *Eur J Biochem* 244(2):279–285.
39. Collins AJ, Schleicher TR, Rader BA, Nyholm SV (2012) Understanding the role of host hemocytes in a squid/vibrio symbiosis using transcriptomics and proteomics. *Front Immunol* 3:91.
40. Bernheim NJ, Dobrogosz WJ (1970) Amino sugar sensitivity in *Escherichia coli* mutants unable to grow on *N*-acetylglucosamine. *J Bacteriol* 101(2):384–391.
41. McCann J, Stabb EV, Millikan DS, Ruby EG (2003) Population dynamics of *Vibrio fischeri* during infection of *Euprymna scolopes*. *Appl Environ Microbiol* 69(10):5928–5934.
42. Wolfe AJ (2005) The acetate switch. *Microbiol Mol Biol Rev* 69(1):12–50.
43. Krulwich TA, Sachs G, Padan E (2011) Molecular aspects of bacterial pH sensing and homeostasis. *Nat Rev Microbiol* 9(5):330–343.
44. Nyholm SV, Stewart JJ, Ruby EG, McFall-Ngai MJ (2009) Recognition between symbiotic *Vibrio fischeri* and the haemocytes of *Euprymna scolopes*. *Environ Microbiol* 11(2):483–493.
45. Flint HJ, Scott KP, Louis P, Duncan SH (2012) The role of the gut microbiota in nutrition and health. *Nat Rev Gastroenterol Hepatol* 9(10):577–589.
46. Guo L, He X, Shi W (2014) Intercellular communications in multispecies oral microbial communities. *Front Microbiol* 5:328.
47. Wolf KJ, et al. (2014) Consumption of acidic water alters the gut microbiome and decreases the risk of diabetes in NOD mice. *J Histochem Cytochem* 62(4):237–250.
48. Troll JV, et al. (2009) Peptidoglycan induces loss of a nuclear peptidoglycan recognition protein during host tissue development in a beneficial animal-bacterial symbiosis. *Cell Microbiol* 11(7):1114–1127.
49. Rader BA, Kremer N, Apicella MA, Goldman WE, McFall-Ngai MJ (2012) Modulation of symbiont lipid A signaling by host alkaline phosphatases in the squid-vibrio symbiosis. *MBio* 3(3):e00093-12.
50. Royet J, Gupta D, Dziarski R (2011) Peptidoglycan recognition proteins: Modulators of the microbiome and inflammation. *Nat Rev Immunol* 11(12):837–851.
51. Bates JM, Akerlund J, Mittge E, Guillemin K (2007) Intestinal alkaline phosphatase detoxifies lipopolysaccharide and prevents inflammation in zebrafish in response to the gut microbiota. *Cell Host Microbe* 2(6):371–382.
52. Lardner A (2001) The effects of extracellular pH on immune function. *J Leukoc Biol* 69(4):522–530.
53. Foster JW (1999) When protons attack: Microbial strategies of acid adaptation. *Curr Opin Microbiol* 2(2):170–174.
54. Merrell DS, Camilli A (1999) The *cadA* gene of *Vibrio cholerae* is induced during infection and plays a role in acid tolerance. *Mol Microbiol* 34(4):836–849.

Supporting Information

Schwartzman et al. 10.1073/pnas.1418580112

SI Materials and Methods

General Procedures. Bacterial strains and plasmids used in this work are listed in Table S2. All *Vibrio fischeri* mutant strains are derived from isolate ES114 (1, 2). *V. fischeri* and *Vibrio harveyi* cells were grown at 28 °C, with shaking at 225 rpm, unless otherwise noted. In *V. fischeri* culture experiments, 5 μg erythromycin (Em)·mL^{-1} or 100 μg kanamycin (Kn)·mL^{-1} were added where indicated. *V. fischeri* cultures were grown in high-osmolarity seawater tryptone medium (SWTO) (3), Luria–Bertani salt medium (LBS) (4), or minimal salts medium (MSM). *Escherichia coli* was cultured at 37 °C with shaking at 250 rpm in Luria–Bertani medium (LB) (5) or M9 minimal medium (6). Where indicated, 50 mM Pipes buffer (pH 7.5), 150 μg Em·mL^{-1}, or 50 μg Kn·mL^{-1} was added to *E. coli* cultures.

Adult squid, collected at Oahu, Hawaii, were maintained in the laboratory in circulating 35-ppt Instant Ocean (Aquarium Systems), on a 12-h/12-h light/dark cycle. Squid were colonized and raised as described previously (7, 8), with the following modifications: Animals were exposed to ∼5,000 colony-forming units (cfu)/mL of the indicated *V. fischeri* strains in filter-sterilized Instant Ocean for 16 h, euthanized, and frozen at −80 °C. Animals were anesthetized for 5 min in seawater containing 2% (vol/vol) ethanol for collection of blood and tissue samples. The mature light-organ developmental state was distinguished in living animals by (*i*) a mantle length of >10 mm and (*ii*) a behavioral transition of the animals to a pattern of nocturnal activity. All animal experiments meet the regulatory standards established for invertebrates by the University of Wisconsin–Madison.

***Es*Chit1 Antibody Design and Validation.** A polyclonal rabbit antibody against the squid chitotriosidase 1 (*Es*Chit1; Genscript) was generated to the synthetic peptide sequence (CYPGSRGSPAVDKKN) that is predicted to be located at an internal, but surface-exposed, portion of the protein (Fig. S5) and that lacked any significant match to other sequences in the squid databases. To determine the specificity of the anti-*Es*Chit1antibody (α-*Es*Chit1), we performed a Western blot analysis, as previously described (9). The protocol was modified so that proteins were transferred to a 0.2-μm nitrocellulose membrane and blocked overnight in a solution containing 4% (wt/vol) milk in 0.1% Tween-20 in Tris-buffered saline (TBS) (20 mM Tris with 0.5 M NaCl, pH 7.4) at 4 °C. After blocking, the membranes were incubated for 3 h at room temperature in 4% milk in 0.1% Tween-20, with either a 1:250 dilution of α-*Es*Chit1 or purified rabbit IgG at the same concentration as a negative control. Secondary antibody and detection of antibody hybridization were performed as described elsewhere (9). This antibody was highly specific relative to an Ig control by Western blot against light-organ central-core tissues, at a concentration of 1:250 (Fig. 2*B*), and was also used for immunochemistry at this concentration (10, 11).

Immunocytochemistry, Fluorescence Microscopy, and Hemocyte Characterization. Fluorochromes were obtained from Life Technologies, and all other chemicals were purchased from Sigma-Aldrich, except where indicated. Immunocytochemistry (ICC) and processing of squid tissues were performed as described previously (10), with minor modifications, described below. All samples were mounted in Vectashield (Vector Laboratories) before observation by confocal microscopy. A Zeiss 510 laser-scanning confocal microscope with AxioImager software (Carl Zeiss Instruments) was used to image samples, unless otherwise noted.

Collection of adult central-core tissue, juvenile light organs, and hemocytes. Central-core tissue was collected from squid >18 mm in mantle length. The light organ was exposed by ventrally dissecting the mantle and removing the funnel. The central cores are located bilaterally on the light organ, in a pocket defined by layers of ink sac and reflector (Fig. 1*A*). The lobes of the organ are surrounded by vitreous lens tissue. To expose the central-core tissue, the lens was dissected just above where the ink sac and reflective tissue fold around the central core, located on the outer edge of the light organ. Weak connective tissue joins the tissue folds between which the central core is located. If this tissue could be removed to fully unfold the reflector and ink sac, then the central core was removed immediately and incubated in a fixative containing 4% (vol/vol) paraformaldehyde (PFA) in mPBS (50 mM sodium phosphate, pH 7.4, 0.4 M NaCl) for 16 h at 4 °C to stabilize the tissues. If the central-core tissue could not be removed without compromising its structural integrity, then the whole light organ was removed from the squid's mantle cavity by cutting the connective tissues underneath the organ, as well as the gut and ligaments attaching it from above, and placing the organ in 4% PFA in mPBS for 5 min, before removal of central-core tissues. Fixed samples were rinsed three times for 10 min in mPBS and then permeabilized 24 h in 1% Triton-X100 in mPBS. Immature light organs were collected as described elsewhere, with minor modifications (11). The light-organ ink sac was gently punctured during dissection to permit drainage of ink and better visualization of deep crypt structures. Hemocyte isolation was performed as described previously (12). Briefly, 15-μL samples of squid hemolymph, extracted from the cephalic vessel, were applied to glass coverslips, and hemocytes were allowed to adhere for 30 min. Following this step, the slides were rinsed three times in Squid Ringer's buffer [530 mM NaCl, 10 mM KCl, 25 mM $MgCl_2$, 10 mM $CaCl_2$, and 10 mM Hepes buffer, pH 7.5 (13)] to remove nonadherent cells, and the samples were fixed for 30 min in 4% PFA in mPBS and permeabilized for 30 min in 1% Triton-X100 in mPBS (mPBST).

Detection of chitin and hemocytes by fluorescent probes. Immature light organs, or central-core tissue, were incubated for 7 d in a 1:250 dilution of TRITC-conjugated chitin-binding protein (CBP) (New England Biolabs) in mPBST (12). To counterstain, tissues were incubated 4 d in a 1:40 dilution of FITC-conjugated DNase-I to visualize hemocytes by their enrichment in globular actin (14) and 25 μg/mL Alexa-633 phalloidin in for 2 d to visualize the actin cytoskeleton. Hemocytes were incubated at room temperature for 3 h with 1:250 FITC-conjugated CBP in mPBST, rinsed, and counterstained with 1:40 rhodamine phalloidin in mPBST overnight at 4 °C to visualize the actin cytoskeleton. A 1:500 dilution of TOTO-3 iodide was added for 10 min at room temperature to visualize nuclear DNA.

Detection of predicted squid chitinases by immunocytochemistry. Permeabilized central-core tissues were incubated at 4 °C with mPBST block (0.5% goat serum and 1% BSA in mPBST) overnight and then for 7 d with a 1:500 dilution of α-*Es*Chit1 primary antibody, or the same concentration of purified rabbit IgG as a negative control, in mPBST block. To visualize antibody binding, samples were incubated overnight in a 1:40 dilution of TRITC-conjugated goat anti-rabbit/chicken secondary antibody. Tissues were counterstained in mPBST for 4 d in a 1:40 dilution of FITC-conjugated DNase-I and overnight with 25 μg Alexa-633 phalloidin per milliliter. Hemocytes were incubated at room temperature in mPBST block for 1 h, then in primary antibody in mPBST block for 3 h, and finally in a 1:40 dilution of FITC-conjugated goat anti-rabbit in mPBST blocking solution

for 45 min. Samples were counterstained overnight at 4 °C with a 1:40 dilution of rhodamine phalloidin in mPBST and for 10 min at room temperature with a 1:500 dilution of TOTO-3 iodide to visualize nuclear DNA.

Enumeration of hemocytes in immature light organs and visualization of mature central-core tissue. To enumerate hemocytes present in immature light organs, samples stained with FITC-DNase-I and rhodamine phalloidin, as described above, were visualized by confocal microscopy. Hemocytes, defined as DNase-I positive cells, were enumerated in a region of the light organ extending from the midaxis line to the ciliated epithelial field. Hemocytes present in the anterior and posterior appendages (structures characteristic of the immature light organ and not present in the fully mature structure) were not enumerated in this analysis. To visualize fluorescently labeled structure in central-core tissue, we located a field of view where the tissue surface was relatively uniform (i.e., the surface tissue had not been disrupted by dissection). Although the boundaries of crypts could not be definitively identified with the fluorescent probes used, we analyzed fields of view where phalloidin, which stains the actin cytoskeleton, formed a honeycomb-like structure, reminiscent of the finger-like projections of the mature light-organ crypt (Fig. 1*A*).

Collection and characterization of expelled crypt contents. To collect crypt contents, anesthetized squid were exposed to a light cue to induce venting behavior, as described previously (15). Acidic compartments of these cells were labeled by staining for 30 min with a 1:500 diution of Lysotracker Red in Squid Ringer's buffer and visualized by epifluorescence microscopy. To assess nuclear-membrane integrity, cells were stained for 5 min with a 1:10,000 dilution of acridine orange and visualized by confocal microscopy. For analysis of chitin and immunocytochemistry, the expelled crypt contents were collected with a negative-pressure pipette and placed directly in 4% PFA in mPBS for 4 h. A 20-μL sample of whole hemolymph was also collected as a control to compare cell morphology and staining patterns. Samples were suspended in Histogel matrix (Richard-Allen Scientific; HG-4000-012) and then embedded in paraffin and cut into 5-μm sections. The sections were deparaffinized and stained with hematoxylin and eosin to identify hemocytes (16). Embedding, sectioning, and staining were performed by the Histology Core Facility in the Surgery Department at the University of Wisconsin–Madison School of Medicine and Public Health. Unstained sections were also processed for fluorescence microscopy and immunocytochemistry, using a previously developed protocol (9). The same concentrations of fluorochromes and antibodies were used as described for staining central-core tissue, light organs, and hemocytes.

Morphological changes of hemocytes exposed to crypt contents. To characterize acidic compartments in hemolymph-derived hemocytes upon exposure to the light-organ crypt contents, hemocytes were collected, incubated with Lysotracker Red as described above, and then centrifuged at 15,800 × *g* for 10 min at 4 °C in a tabletop centrifuge to remove excess dye. The cells were resuspended in Squid Ringer's buffer adjusted to either pH 7.5 or pH 5.5 [the nocturnal crypt pH (9)]. Fresh crypt contents were collected from the same animal and placed on ice. When the hemolymph-derived hemocytes had been labeled, 5 μL of fresh crypt contents was added to 20 μL of labeled hemocytes in either pH 7.5 or pH 5.5 buffer. The remaining crypt contents were heated to 95 °C for 10 min, to inactivate heat-labile crypt-contents components. Five microliters of heat-exposed crypt contents were added to 20 μL of Lysotracker-Red–labeled cells in pH 7.5 buffer. Samples were incubated for 2 h and then visualized using a Zeiss Axio Imager M2 epifluorescence microscope. To ensure that morphological irregularities were not a result of experimental manipulations, a control population of hemocytes was collected and processed in the same manner as that of the experimental samples, except that the hemocytes were not exposed to crypt contents.

RNA Extraction, Sequence Characterization, and Quantitative RT-PCR. The full-length *eschit1* transcript was obtained by RACE amplification, as described previously (9) (Fig. S5). The sequence was deposited in GenBank (accession no. KM592978). cNA synthesized from juvenile light organ total RNA was used as the template. The sample collection and transcriptional analysis were performed as described previously (9). Three-day-old and 4-wk-old light organs collected at 2 h, 10 h, and 22 h postdawn (hpd) were dissected in RNAlater (either $n = 4$ replicates of 20 juvenile light organs per replicate or $n = 4$ replicates of 5 adult light organs per replicate). To correct for the presence of bacterial symbiont RNA in the samples, amounts of total RNA added to the cDNA synthesis reactions were scaled, as follows: 2 hpd, 1×; 10 hpd, 1.1×; 22 hpd, 1.2×. Primer-set efficiencies were between 95% and 105% as determined by standard curves, using 10-fold dilutions of template. Primers are listed in Table S3. A 60 °C annealing temperature was used for all primer pairs. Candidate gene expression was normalized using the geometric mean of 40S ribosomal RNA and serine hydroxymethyltransferase (serine HMT) expression values. The distribution of the data was measured by Shapiro's test (all data fitted a normal distribution), and a two-way ANOVA with post hoc Bonferroni comparison was used to compare gene expression among time points and between colonization states.

Quantitative RT-PCR procedures were conducted in accordance with the MIQE guidelines (17) for sample collection, RNA isolation, cDNA synthesis, quantitative RT-PCR amplification, normalization of experimental gene expression using reference genes, and data analysis. Primers were designed by OligoAnalyzer software (Integrated DNA Technologies) (Table S2).

Molecular Genetics. All plasmids were constructed and introduced into *V. fischeri* with standard molecular techniques (18). To construct a vector for *in trans* complementation of the *nagB* gene deletion, a segment of DNA corresponding to 500 bp upstream and 100 bp downstream of the annotated *nagB* coding sequence was amplified using primers with unique restriction sites engineered at the 5′ end and cloned into the *V. fischeri* Tn*7*-site integration plasmid, pEVS107 (18) (Table S2). The plasmid was introduced into the appropriate *V. fischeri* strain by conjugative transfer and integrated into the Tn*7* locus with the help of the pUXBF13 plasmid, as previously described (18–20) (Table S2).

Growth-Yield Measurement. To assess growth on a sole source of carbon, strains were cultivated for 24 h in MSM (21), modified as described previously (22). The medium was buffered at pH 7.5 with 50 mM Pipes and contained either 5 mM di-*N*-acetyl chitobiose (Cayman Chemicals) or 10 mM *N*-acetylglucosamine, glucosamine, or glucose. Strains were first grown as LBS cultures and then subcultured 1:100 into 0.2% casamino acids in MSM until they reached an optical density (600 nm, 1 cm path length, OD_{600}) of 0.40 ± 0.05 absorbance units. These cultures were used to inoculate (at a dilution of 1:100) MSM supplemented with a single carbon source. Optical density was determined after 36 h of growth.

Acid Tolerance Assays. Induction of acid tolerance in *V. fischeri* was assessed using a modified version of the acid-killing assays developed for *Vibrio cholerae* (23). To measure induction of acid tolerance in cultured cells, 30-mL SWTO cultures of *V. fischeri* were grown in 125-mL flasks with shaking to an OD_{600} of 0.4 ± 0.05. Cells were harvested by centrifugation for 6 min at 5,000 × *g*. To measure the potential for cells to adapt to a sublethal amount of organic-acid stress, 90% of the cells were resuspended in 0.5 mL SWTO (pH 5.5) containing 50 mM Pipes and 0.075× organic

acids (1× organic acids = 74 mM propionic acid, 174 mM acetic acid, and 50 mM butyric acid). The remaining 10% of the cells were resuspended in 0.5 mL SWTO (pH 7.5) containing 50 mM Pipes without organic acids. Cell suspensions were incubated for 1 h at 28 °C with shaking, before centrifugation, and pellet resuspension in 0.5 mL SWTO (pH 4.75) containing 0.1× organic acids and 50 mM Pipes. Aliquots of cells (20 μL) were removed at 10-min intervals and serially diluted, and 10 μL of each dilution was spotted onto LBS agar plates for colony enumeration. Percentage survival at time T_n was calculated by (cfu/mL)T_n − (cfu/mL)T_0 × 100. To assay for induction of acid tolerance by catabolism of COS, cells were grown in 30 mL of 20 mM COS in SWTO (pH 7.5) with and without an additional 50-mM Pipes buffer, pelleted, and resuspended directly in SWTO (pH 4.75) containing 50 mM Pipes and 0.1× organic acids.

To assay the induction of acid tolerance in symbiotic cells of *V. fischeri*, symbiont-containing tissues (from mature squid with mantle length >15 mm), whole light organs (from squid with 10–15 mm mantle length) or batches of 50 whole light organs (from juvenile squid with <10 mm mantle length) were gently homogenized to release bacterial cells. Symbiont-containing supernatant from the light-organ homogenate was pelleted by centrifugation, and survival was compared between populations resuspended directly in lethal SWTO (pH 4.75) containing 50 mM Pipes and 0.1× organic acids or following a 1-h incubation under the inducing condition of SWTO (pH 5.5) containing 50 mM Pipes and 0.075× organic acids.

Acetate and Glucose Detection. Samples of *V. fischeri*, *V. harveyi*, or *E. coli* culture supernatant were assayed for acetate production and glucose consumption: Cells were grown in 3 mL LBS (*Vibrio* spp.) or LB (*E. coli*) broth to OD_{600} of 0.5 ± 0.05, and 0.25 mL of these cultures was pelleted, rinsed, and resuspended in 3 mL of MSM (for *Vibrio* spp.) (21) or M9 (for *E. coli*) (24) containing either 5 mM GlcNAc or 5 mM glucose. MSM and M9 are both minimal media, containing similar profiles of minerals, at different compositions. These media have been previously optimized for the growth of marine (MSM) or terrestrial (M9) microbes. Cultures were grown with shaking in 18-mm test tubes at 225 rpm for 2 h. To determine the level of acetate accumulation in the minimal medium supernatant, 100-μL aliquots of bacterial cultures at an OD_{600} of 0.5 ± 0.05 were centrifuged for 15 min at 13,000 × *g* and 4 °C to remove cells. The cell-free supernatant was stored at −20 °C until assayed. A coupled-enzyme assay (Sigma-Aldrich; no. MAK086) was used to detect acetate, following the manufacturer's protocol. Absorbance at 420 nm was monitored to detect the accumulation of the colorimetric substrate with a TECAN plate reader and Magellan automation software (Tecan Group). The concentration of acetate in the culture supernatant was calculated based on a linear regression of measurements for acetate standards of known concentration (R^2 = 0.93, over a range of 0–300 μM). Where necessary, samples were diluted to fall within the detection limits of the assay. The amount of acetate per cell was divided by the OD_{600} to normalize between conditions. Glucose was detected by a glucose-oxidase coupled-enzyme assay (Sigma-Aldrich; no. GAGO20), following the manufacturer's protocol. Absorbance at 600 nm was monitored to detect *o*-dianisidine, the colorimetric product, proportional to the original glucose concentration. The concentration of glucose in the culture supernatant was calculated by a comparison with a calibration curve generated from standards of known glucose concentration (R^2 = 0.99, over a range of 0–500 μM glucose). Samples were diluted as necessary to fall within the linear range of glucose concentration detected by the assay, as defined by the calibration curve.

Hemolymph Titration. To determine the buffering capacity of hemolymph, 100-μL samples of cell-free hemolymph were first diluted 1:10 in deionized water and then titrated with 0.1 M HCl. pH measurements were made using an Orion PerpHect LogR meter and a Silver/Silver Chloride reference electrode (ThermoFisher Scientific).

SI Calculations

Calculations in Support of COS Delivery by Hemocytes. Assumptions and measured quantities:

i) It takes ∼7.5 mM acetate to acidify hemolymph to pH 5.5 (Fig. S4*E*).
ii) The theoretical yield of acetate is three molecules of acetate per molecule of GlcNAc.
iii) Because COS are made of GlcNAc monomers, these calculations are done assuming GlcNAc is the form of COS.
iv) The molecular weight of GlcNAc is 221 g/mol.
v) The crypt contents are ∼20 μL and contain 10^3–10^4 hemocytes (15).
vi) The density of GlcNAc is 1.5 g/cm^3.
vii) The hemolymph is approximately pH 7 (9).

About How Much COS Would It Take to Acidify the Light Organ?

i) It takes ∼7.5 mM acetate to acidify hemolymph from pH 7 to pH 5.5 (Fig. S4*E*).
Assume that the volume acidified is ∼20 μL hemolymph (vented volume) (15) and that acetate is the major acidic component:

$$7.5\times10^{-3}\ \text{mol acetate/L} * 20\times10^{-6}\text{L} = 1.5\times10^{-7}\ \text{mol acetate}$$

$$1.5\times10^{-7}\ \text{mol acetate} * 1\ \text{mol COS}/3\ \text{mol acetate} = \sim 5\times10^{-8}\ \text{mol COS/light organ}$$

$$5\times10^{-8}\ \text{mol COS/light organ} * 221\ \text{g/mol} = \sim 11\ \mu\text{g COS/light organ.}$$

Although the epithelial cells could take up acetate (pK_a 4.76), 75% of the acetate will carry a negative charge when the nocturnal crypt pH is 5.5, suggesting that unless acetate uptake is an active process, the amount of protonated acetate lost from the crypt lumen by epithelial absorption will be small.

ii) COS cannot be present at concentrations much greater than 2.5 mM at one time, because the cocolonization of *ΔnagB* and wild type is not biased toward wild type (Fig. S3 *D* and *E*).
A total of 2.5 mM COS is equivalent to 11 μg in a 20-μL crypt volume.

About How Many Hemocytes Would It Take to Deliver This Amount of COS? If each hemocyte releases eight 1-μm diameter spherical granules of COS,

$$\text{The volume of the chitin granule} = \sim 5\times10^{-10}\ \text{cm}^3.$$

$$1.5\ \text{g/cm}^3 * 5\times10^{-10}\ \text{cm}^3 = 7.5\times10^{-10}\ \text{g/granule} * 8\ \text{granules/cell} = \sim 6\times10^{-3}\mu\text{g GlcNAc per cell.}$$

This means that the calculated 11 μg COS could be delivered by ∼2,000 hemocytes.

Previous quantification of hemocytes in crypt contents was estimated at 10^3–10^4 hemocytes per light-organ crypt (15).

1. Boettcher KJ, Ruby EG (1990) Depressed light emission by symbiotic *Vibrio fischeri* of the sepiolid squid *Euprymna scolopes*. *J Bacteriol* 172(7):3701–3706.
2. Mandel MJ, Stabb EV, Ruby EG (2008) Comparative genomics-based investigation of resequencing targets in *Vibrio fischeri*: Focus on point miscalls and artefactual expansions. *BMC Genomics* 9:138.
3. Stabb EV, Butler MS, Adin DM (2004) Correlation between osmolarity and luminescence of symbiotic *Vibrio fischeri* strain ES114. *J Bacteriol* 186(9):2906–2908.
4. Graf J, Dunlap PV, Ruby EG (1994) Effect of transposon-induced motility mutations on colonization of the host light organ by *Vibrio fischeri*. *J Bacteriol* 176(22):6986–6991.
5. Sambrook J, Fritsch EF, Maniatis T (1989) *Molecular Cloning* (Cold Spring Harbor Lab Press, Cold Spring Harbor, NY).
6. Miller JH (1972) *Experiments in Molecular Genetics* (Cold Spring Harbor Lab Press, Cold Spring Harbor, NY).
7. Lynn MN, Mark JM (2012) Colonization of *Euprymna scolopes* squid by *Vibrio fischeri*. *J Vis Exp* 61:e3758.
8. Koch EJ, Miyashiro T, McFall-Ngai MJ, Ruby EG (2014) Features governing symbiont persistence in the squid-vibrio association. *Mol Ecol* 23(6):1624–1634.
9. Kremer N, et al. (2014) The dual nature of haemocyanin in the establishment and persistence of the squid-vibrio symbiosis. *Proc Biol Sci* 281(1785):20140504.
10. Troll JV, et al. (2009) Peptidoglycan induces loss of a nuclear peptidoglycan recognition protein during host tissue development in a beneficial animal-bacterial symbiosis. *Cell Microbiol* 11(7):1114–1127.
11. Kremer N, et al. (2013) Initial symbiont contact orchestrates host-organ-wide transcriptional changes that prime tissue colonization. *Cell Host Microbe* 14(2):183–194.
12. Heath-Heckman EA, McFall-Ngai MJ (2011) The occurrence of chitin in the hemocytes of invertebrates. *Zoology* 114(4):191–198.
13. Nyholm SV, Stewart JJ, Ruby EG, McFall-Ngai MJ (2009) Recognition between symbiotic *Vibrio fischeri* and the haemocytes of *Euprymna scolopes*. *Environ Microbiol* 11(2):483–493.
14. Altura MA, et al. (2013) The first engagement of partners in the *Euprymna scolopes-Vibrio fischeri* symbiosis is a two-step process initiated by a few environmental symbiont cells. *Environ Microbiol* 15(11):2937–2950.
15. Nyholm SV, McFall-Ngai MJ (1998) Sampling the light-organ microenvironment of *Euprymna scolopes*: Description of a population of host cells in association with the bacterial symbiont *Vibrio fischeri*. *Biol Bull* 195(2):89–97.
16. Sheehan DC, Hrapchak BB (1980) *Theory and Practice of Histotechnology* (Mosby, St Louis).
17. Bustin SA, et al. (2009) The MIQE guidelines: Minimum information for publication of quantitative real-time PCR experiments. *Clin Chem* 55(4):611–622.
18. McCann J, Stabb EV, Millikan DS, Ruby EG (2003) Population dynamics of *Vibrio fischeri* during infection of *Euprymna scolopes*. *Appl Environ Microbiol* 69(10):5928–5934.
19. Bao Y, Lies DP, Fu H, Roberts GP (1991) An improved Tn7-based system for the single-copy insertion of cloned genes into chromosomes of gram-negative bacteria. *Gene* 109(1):167–168.
20. Stabb EV, Ruby EG (2002) RP4-based plasmids for conjugation between *Escherichia coli* and members of the Vibrionaceae. *Methods Enzymol* 358:413–426.
21. Adin DM, Visick KL, Stabb EV (2008) Identification of a cellobiose utilization gene cluster with cryptic β-galactosidase activity in *Vibrio fischeri*. *Appl Environ Microbiol* 74(13):4059–4069.
22. Miyashiro T, et al. (2011) The *N*-acetyl-D-glucosamine repressor NagC of *Vibrio fischeri* facilitates colonization of *Euprymna scolopes*. *Mol Microbiol* 82(4):894–903.
23. Merrell DS, Camilli A (1999) The *cadA* gene of *Vibrio cholerae* is induced during infection and plays a role in acid tolerance. *Mol Microbiol* 34(4):836–849.
24. Anonymous (2010) M9 minimal medium (standard). *Cold Spring Harb Protoc* 2010(8): pdb.rec12295.

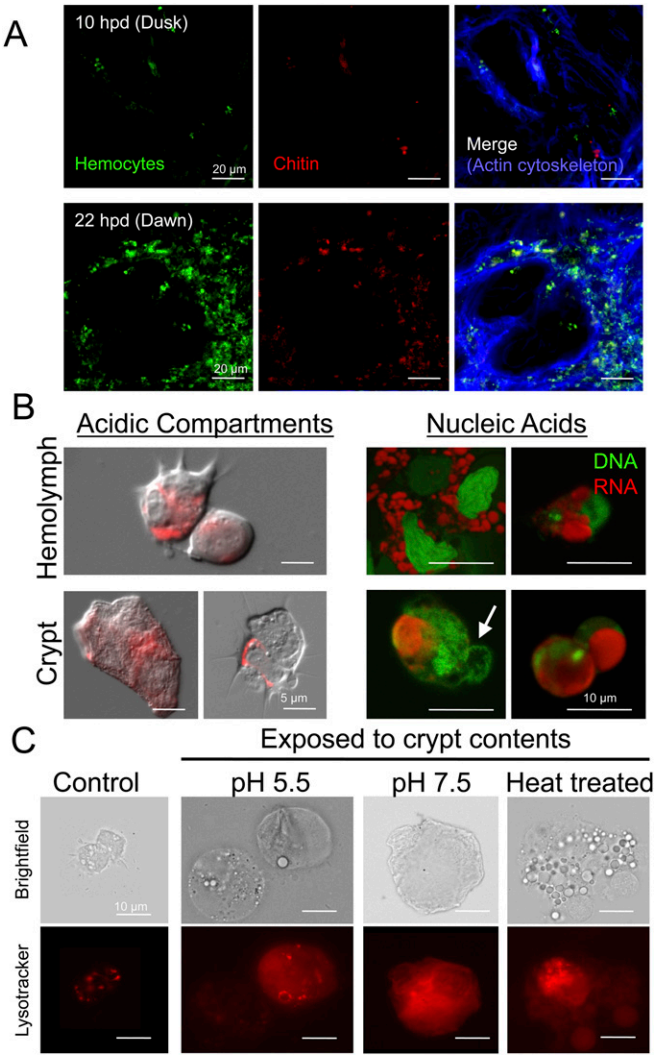

Fig. S1. Presence of chitin and hemocytes in light-organ tissue and morphological changes of hemocytes exposed to the light-organ crypt environment. (*A*) Confocal micrographs, showing colocalization of fluorescently labeled hemocyte-specific marker DNase-I (green, FITC label, binds globular actin) and chitin-specific chitin-binding protein (red, TRITC label, binds particulate chitin). Actin-rich extracellular matrix was detected with Alexa 633 phalloidin (blue). Tissue was sampled at dusk (*Top*, 10 h postdawn, hpd) and before dawn (*Bottom*, 22 hpd). (*B*, *Left*) Morphology of hemocytes derived from the squid hemolymph (*Top*) and the light-organ crypt (*Bottom*). Images are merged differential interference contrast and fluorescent micrographs. Acidic compartments within cells were labeled with Lysotracker Red. (*Right*) DNA (green) and RNA (red) were labeled with acridine orange. Arrow indicates irregular nuclear morphology. (*C*) Morphological changes are induced in hemocytes upon exposure to crypt contents. Hemolymph (containing hemocytes) and crypt contents were collected from a single animal at 22 hpd. (*Left*) The acidic vesicles of these hemocytes were labeled with Lysotracker Red. The labeled cells were then exposed to 25% crypt contents in pH 5.5, the nocturnal pH of the crypt (1), in Squid Ringers buffer, and monitored over time. (*Center Left*, *Center Right*, and *Right*) Blebbing of the hemocyte cell membrane and loss of vacuolar integrity, indicated by diffuse Lysotracker staining, were observed after 1 h of exposure to crypt contents. Similar results were obtained when the hemocytes were exposed to either 25% heat-treated crypt contents or 25% crypt contents in pH 7.5 Squid Ringer's buffer.

1. Kremer N, et al. (2014) The dual nature of haemocyanin in the establishment and persistence of the squid-vibrio symbiosis. *Proc Biol Sci* 281(1785):20140504.

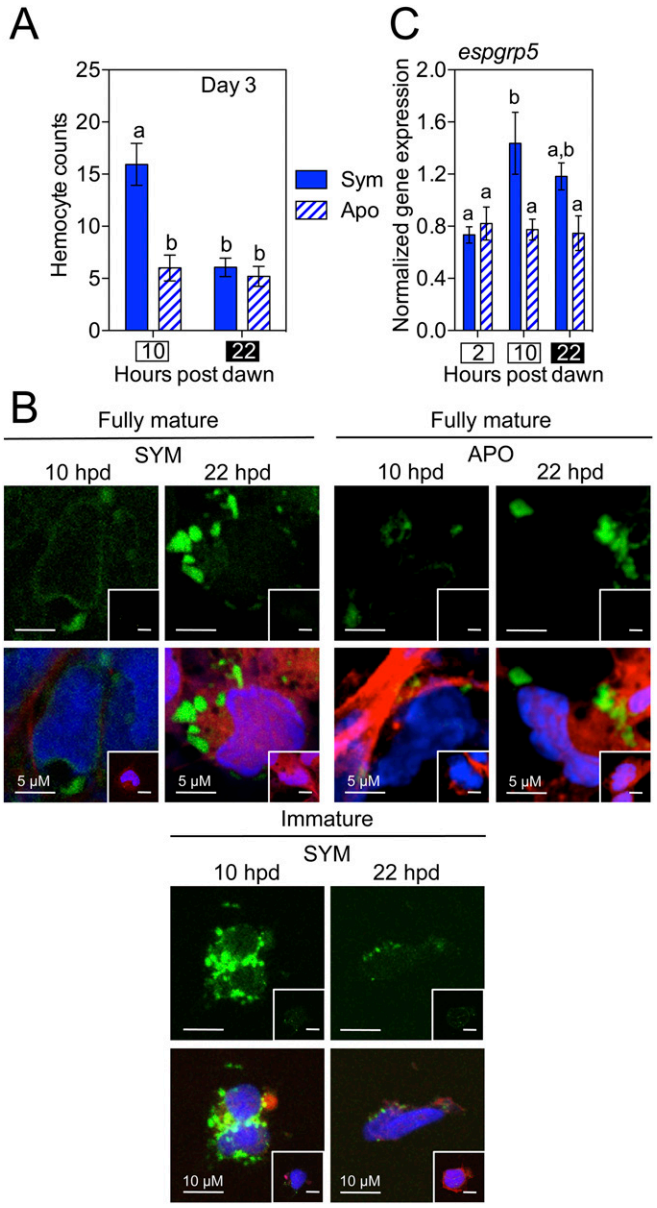

Fig. S2. Diel hemocyte-associated phenotypes. (*A*) Diel migratory behavior of hemocytes in symbiotic (Sym) or aposymbiotic (Apo) 3-d-old light organs, assessed during the day (white box) and night (black box). Data represent two independent experiments. "a" and "b" denote groups of statistically similar means, assessed by two-way ANOVA with post hoc Bonferroni *T*-tests. (*B*) Detection of *Es*Chit1-positive granules in hemocytes derived from symbiotic (SYM) and aposymbiotic (APO) squid 10 h and 22 h postdawn (hpd). *Insets* show the corresponding preimmune controls. (*Top*) Hemocytes were isolated from individual fully mature squid (>4 wk old). Observations were made from three independent samples. (*Bottom*) Detection of *Es*Chit1 in hemocytes isolated from pools of 15 immature squid (2 d posthatch). Images represent observations from two independent samples. (*C*) Transcription of the hemocyte-associated gene *espgrp5* (1) in 4-wk-old light organs measured during the day (white boxes), or at night (black box). Bars represent SEM, $n = 4$. a and b indicate groups of statistically similar means, assessed by two-way ANOVA with post hoc Bonferroni *T*-tests.

1. Collins AJ, Schleicher TR, Rader BA, Nyholm SV (2012) Understanding the role of host hemocytes in a squid/vibrio symbiosis using transcriptomics and proteomics. *Front Immunol* 3:91.

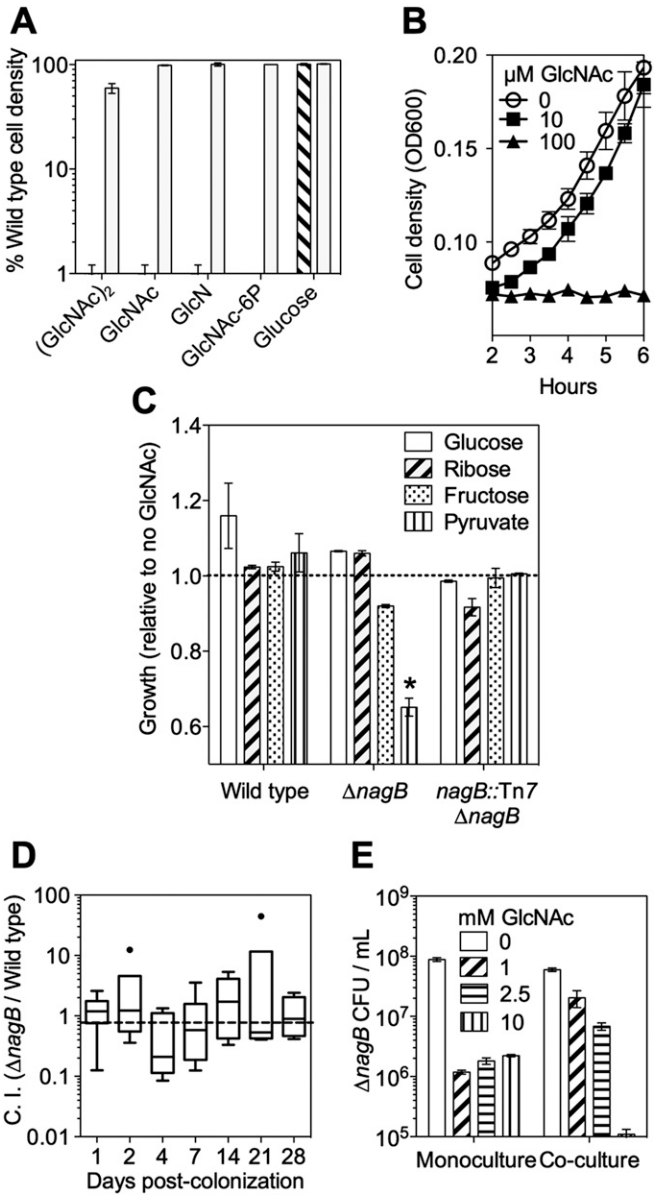

Fig. S3. Phenotypes of the COS biosensor strain, *ΔnagB*. (*A*) Growth of *ΔnagB* (hatched bar) and an *in cis* genetic complement, *ΔnagB* Tn*7*::*nagB* (open bars), relative to wild-type *V. fischeri* on different sugars. $(GlcNAc)_2$, chitobiose; GlcNAc, *N*-acetylglucosamine; GlcN, glucosamine. Bars indicate SEM, $n = 2$. (*B*) Concentration dependence of COS sensitivity. Cultures were grown in LBS with added GlcNAc, and growth was measured by optical density at 600 nm (OD_{600}). Bars indicate SEM, $n = 3$. (C) Ability of nongluconeogenic carbohydrates to reverse *ΔnagB* substrate inhibition. Growth of wild type, *ΔnagB*, and *ΔnagB* Tn*7*::*nagB* was assessed in the presence of both GlcNAc and the indicated, non-COS, carbohydrate. The capacity of the second carbohydrate to functionally complement substrate inhibition by GlcNAc was assessed by comparison with growth on the carbohydrate in the absence of GlcNAc. Bars indicate SEM, $n = 3$; * indicates a mean ratio of growth in the presence vs. absence of GlcNAc statistically different from 1.0, assessed by one-sample *T*-test. (*D*) Four-week co-colonization with both *ΔnagB* and wild-type *V. fischeri*. C.I., competitive index. Center bar indicates median C.I., inner fences are determined by Tukey's method, and outliers are shown as solid circles, $n = 6$ squid per time point. (*E*) Growth of *ΔnagB* with COS in complex medium. The *ΔnagB* strain was either cultured alone (monoculture) or cocultured with wild-type *V. fischeri* at an initial inoculum of 1:1. Bars indicate SEM, $n = 6$.

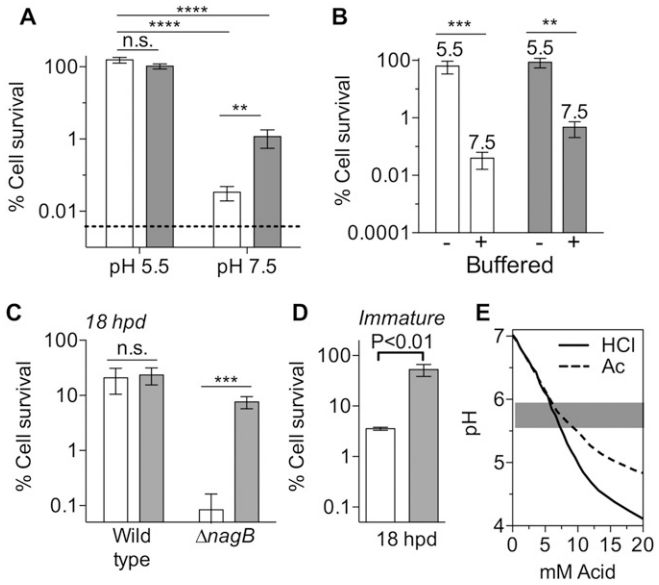

Fig. S4. Characterization of the conditions sufficient to induce the *V. fischeri* acid tolerance response and acidify the light-organ crypt. Throughout, bars indicate SEM, groups of statistically different means, determined by two-way ANOVA with post hoc Bonferroni *T*-tests. $*P < 0.05$, $**P < 0.01$, $***P < 0.005$, $****P < 0.001$; n.s., no significance. (*A–D*) Induction of acid tolerance was measured by calculating the survival of *V. fischeri* for 20 min in 0.1× organic acids medium (pH 4.75). *(A) V. fischeri* was grown either in pH 5.5 or in pH 7.5 media in the absence (open bars) or presence (solid bars) of 0.075× organic acids **(***n* = 4). (*B*) Induction of acid tolerance during growth of wild-type (open bars) or *ΔnagB* (solid bars) *V. fischeri* on 20 mM glucose in LBS medium. Medium was either buffered at pH 7.5 with 50 mM Pipes or left unbuffered. Final pH of the culture medium before killing challenge is noted above the bars (*n* = 4). (*C*) Symbiotic wild-type or *ΔnagB V. fischeri* were released from mature light organs at night (18 h postdawn, hpd). Released symbionts were assayed for their survival upon immediate acid exposure (open bars) or after preexposure to pH 5.5 medium containing 0.075× organic acids (solid bars) to compare the potential for induction of acid tolerance (*n* = 5). (*D*) Induction of acid tolerance of wild-type *V. fischeri* released from a pool of 20 2-d-old light organs at night (18 hpd) and assayed immediately for survival (open bar). A portion of the released cells was incubated for 1 h in 0.075× organic acids medium (pH 5.5) as a positive control for the capacity to induce acid tolerance (solid bar) (*n* = 2). *P* value was determined by two-tailed *T*-test. (*E*) Buffering capacity of cell-free squid hemolymph was determined by titration with either hydrochloric acid (HCl) or acetic acid (Ac). The pH range previously measured in light-organ crypts at night is indicated in the shaded area (1).

1. Kremer N, et al. (2014) The dual nature of haemocyanin in the establishment and persistence of the squid-vibrio symbiosis. *Proc Biol Sci* 281(1785):20140504.

>*E. scolopes* putative chitotriosidase EsChit1
MASTFATVFGVLSLCFLGLHLTNGEYKKVCYYTNWSQYRQIPAKFVPENISVSLCTHIIY
TFATLQNNHLKPFEWNDDSTPWMVGMYARVMKLKKKDPNLQVLLGVGGWNMGSYL
FSKMVANIQNRKMFYTNATGFLRKRNFDGLDIDWCYPGSRGSPAVDKKNYVSLLQETS
DYFLNESKISGKKRLLLTASIPVGKKTIIKGYDIPQVEKYLDFMNLMSYDYHGGSFDNVT
GHNSPLYPRKEETGDERTFNVNWSANYWVEHGVPRMKLNIGMPAYGRGFRLANHSCIL
PGCPSIGPNSPGQYTRLAGFLAYYEICDLIKKGAKVFRIADQKVPYLVYNNEWIGYDDV
KSLSIKVDWLKKNQFGGVAIWTLDLDDFFNGCGSGAYILIKTLTQELKLPSVEN

Fig. S5. Predicted protein sequence of the putative *Es*Chit1 chitotriosidase. Underlined sequence indicates peptide used for antibody production.

Table S1. Acetate excretion during aerobic growth on a single sugar

Strain	Sugar	mM acetate per OD unit	mM acetate produced per mM glucose used
Vibrio fischeri ES114	GlcNAc	9.8 ± 0.7	—
	Glucose	7.0 ± 0.2	0.9 ± 0.1
V. fischeri MJ11	GlcNAc	**11.9 ± 0.7**	—
	Glucose	**9.1 ± 0.5**	1.2 ± 0.1
Vibrio harveyi B392	GlcNAc	8.7 ± 0.2	—
	Glucose	6.7 ± 0.2	0.9 ± 0.1
Escherichia coli K12 (MG1655)	GlcNAc	**3.6 ± 0.1**	—
	Glucose	**4.0 ± 0.5**	**0.5 ± 0.1**

n = 3; ±, SEM; boldface type indicates a significantly different mean from ES114 on the same sugar. Strains were grown with shaking in minimal medium containing 5 mM GlcNAc (COS) or glucose; all strains grew to about the same yield (OD = 0.6–1.0). pH remained above 6.5 in all strains.

Table S2. Strains and plasmids used in this study

Strain or plasmid	Description	Source
V. fischeri		
ES114	Wild-type *E. scolopes* light-organ isolate	(1, 2)
MJ11	Wild-type isolate from fish, *Monocentris japonica*	(3)
TIM313	ES114 Tn*7*::pEVS107 Em^r	(4)
TIM302	ES114 *Tn7::gfp* Em^r	(4)
JAS101	ES114 Δ*nagB Tn7*::pEVS107 Em^r	(5)
JAS102	ES114 Δ*nagB Tn7*::pJAS102 Em^r	This study
V. harveyi		
B392	Wild-type isolate from seawater	(6)
E. coli		
DH5α-λpir	F^- φ80*lacZ*Δ*M15* Δ(*lacZYFargF*)U169 *supE44 deoR hsdR17 recA1 endA1 gyrA96 thi-1 relA1*, lysogenized with λ*pir*	(7)
K-12 (MG1655)	Wild-type *E. coli* $F^-\lambda$	ATCC47076
Plasmids		
pEVS104	R6Kori RP4 *oriT trb tra* Kn^r	(8)
pUX-BF13	R6Kori *tns bla*	(9)
pEVS107	R6Kori *oriT mini*-Tn*7 mob* Em^r Kn^r	(10)
pJAS102	*nagB::*Tn*7* pEVS107	This study

1. Boettcher KJ, Ruby EG (1990) Depressed light emission by symbiotic *Vibrio fischeri* of the sepiolid squid *Euprymna scolopes*. *J Bacteriol* 172(7):3701–3706.
2. Mandel MJ, Stabb EV, Ruby EG (2008) Comparative genomics-based investigation of resequencing targets in *Vibrio fischeri*: Focus on point miscalls and artefactual expansions. *BMC Genomics* 9:138.
3. Ruby EG, Nealson KH (1976) Symbiotic association of *Photobacterium fischeri* with the marine luminous fish *Monocentris japonica*; a model of symbiosis based on bacterial studies. *Biol Bull* 151(3):574–586.
4. Miyashiro T, Wollenberg MS, Cao X, Oehlert D, Ruby EG (2010) A single *qrr* gene is necessary and sufficient for LuxO-mediated regulation in *Vibrio fischeri*. *Mol Microbiol* 77(6): 1556–1567.
5. Miyashiro T, et al. (2011) The *N*-acetyl-D-glucosamine repressor NagC of *Vibrio fischeri* facilitates colonization of *Euprymna scolopes*. *Mol Microbiol* 82(4):894–903.
6. Reichelt JL, Baumann P (1973) Taxonomy of the marine, luminous bacteria. *Arch Mikrobiol* 94(4):283–330.
7. Hanahan D (1983) Studies on transformation of *Escherichia coli* with plasmids. *J Mol Biol* 166(4):557–580.
8. Stabb EV, Ruby EG (2002) RP4-based plasmids for conjugation between *Escherichia coli* and members of the Vibrionaceae. *Methods Enzymol* 358:413–426.
9. Bao Y, Lies DP, Fu H, Roberts GP (1991) An improved Tn7-based system for the single-copy insertion of cloned genes into chromosomes of gram-negative bacteria. *Gene* 109(1): 167–168.
10. McCann J, Stabb EV, Millikan DS, Ruby EG (2003) Population dynamics of *Vibrio fischeri* during infection of *Euprymna scolopes*. *Appl Environ Microbiol* 69(10):5928–5934.

Table S3. Primers used in this study

Gene	Primer sequences	Amplicon size, bp
Serine hydroxymethyl transferase	SerineHMT-qF: GTCCTGGTGACAAGAGTGCAATGA SerineHMT-qR: TTCCAGCAGAAAGGCACGATAGGT	148 (1)
40S Ribosomal protein S19	40S-qF: AATCTCGGCGTCCTTGAGAA 40S-qR: GCATCAATTGCACGACGAGT	103 (1)
Chitotriosidase 1	*Es*Chit1-qF: CCTGCATATGGACGAGGATTT *Es*Chit1-qR: GTATATTGACCAGGTGAGTTGGG	92
Peptidoglycan recognition protein 5	*Es*PGRP5-qF: TTGGAGCCCACACCAAGTTCTACA *Es*PGRP5-qR: CAAGACAGCAGGCGTTTCAATGCT	NR (2)

NR, not reported in original publication.

1. Wier AM, et al. (2010) Transcriptional patterns in both host and bacterium underlie a daily rhythm of anatomical and metabolic change in a beneficial symbiosis. *Proc Natl Acad Sci USA* 107(5):2259–2264.
2. Collins AJ, Schleicher TR, Rader BA, Nyholm SV (2012) Understanding the role of host hemocytes in a squid/vibrio symbiosis using transcriptomics and proteomics. *Front Immunol* 3:91.